MOLECULAR PHYSICS, 20 JULY 2003, VOL. 101, NO. 14, 2157–2169

Taylor & Francis
Taylor & Francis Group

On the development of a general force field for the molecular simulation of perfluoroethers

H.-C. LI[1], C. MCCABE[2], S. T. CUI[1,3], P. T. CUMMINGS[4,3] and H. D. COCHRAN[3,1]*

[1]Department of Chemical Engineering, University of Tennessee, Knoxville, TN 37996-2200, USA
[2]Department of Chemical Engineering, Colorado School of Mines, Golden, CO 80401-1887, USA
[3]Chemical Sciences Division, Oak Ridge National Laboratory, Oak Ridge, TN 37831-6181, USA
[4]Department of Chemical Engineering, Vanderbilt University, Nashville, TN 37235-1604, USA

(*Received 7 October 2002; revised version accepted 7 May 2003*)

We report the development of a transferable force field for the accurate modelling of perfluoroethers. The potential model takes the general form in which separate bond bending and torsional terms describe the intramolecular interactions, with the addition of van der Waals and electrostatic terms to describe the non-bonded interactions. *Ab initio* quantum mechanical calculations were carried out to obtain the partial charges and intramolecular torsional and bending potentials. The van der Waals interactions are described by Lennard-Jones potentials, the parameters of which are optimized to reproduce the available experimental vapour–liquid equilibrium data. An extension of the Gibbs–Duhem method was used to speed up the optimization.

1. Introduction

Perfluoropolyethers, and perfluoro compounds in general, have a unique combination of physical and chemical properties which makes them suitable for a wide range of potential applications in the medical, biotechnology, electronic, and oil and gas industries [1, 2]. As a result, in the past decade, perfluoroethers have attracted interest from researchers in both industry and academia.

Perfluoropolyethers are generally unreactive, non-toxic, non-flammable fluids, making them excellent candidates for high-performance lubricants [3–5]. For example, Fomblin® and Krytox® are widely used as lubricants for magnetic recording media because of their low vapour pressure, oxidative stability, and relatively stable structures [6–8]. A number of theoretical and experimental studies have focused on the physical properties and chemical reactions of these molecules in applications such as hard disk drive lubrication [9, 10]. In particular, Waltman [11] used *ab initio* and experimental methods to study the mobile state of the lubricants and the interaction of the lubricants with the carbon surface. The energy barrier for rotation about bonds between backbone atoms and the torsional potentials were studied, concluding that rotation around the C–O bond has a lower energy barrier than that around the C–C bond; hence, lubricants with more C–O bonds (in this case, Zdol®) are more flexible.

As with many other polymers, monomers or oligomers of perfluoropolyethers have been used as building blocks in copolymers to adjust the properties of the polymer product by changing the type and ratio of co-monomers [12–16]. One of the important properties of perfluorinated compounds is their extremely low intermolecular interaction, which accounts for many of their distinctive properties, including their low surface tension. For example, the surface tension of perfluoropolyethers is around 20–22 $mN\,m^{-1}$ [12], which is much lower than that of hydrocarbon polymers. By using perfluoropolyethers to form block copolymers with hydrocarbon polymers, the surface properties of the polymer can be adjusted [12] which is of considerable industrial interest.

A particularly topical application is the possible use of functionalized perfluoropolyethers as surfactants that can form microemulsions which disperse water in

*Author for correspondence. e-mail: hdc@ornl.gov

Molecular Physics ISSN 0026–8976 print/ISSN 1362–3028 online © 2003 Taylor & Francis Ltd
http://www.tandf.co.uk/journals
DOI: 10.1080/0026897031000154329

supercritical carbon dioxide [17–19], helping to make CO_2 a more versatile replacement solvent in the chemical and related industries. In 1996, Johnston *et al.* [18] used several spectroscopic techniques to verify the existence of water cores inside reverse micelles formed by an ammonium carboxylate perfluoropolyether with an average molecular weight of 740. They also showed that protein molecules, bovine serum albumin (BSA), dissolved in the water core have spectroscopic properties similar to those dissolved in buffer solution at pH = 7.0 mimicking pure water. This provided strong evidence that the aqueous environment inside the reverse micelles is similar to that of bulk water, which is important for example in enzymatic reactions. Eastoe *et al.* [20] also observed the formation of reverse micelles with a water core in near-critical carbon dioxide with a di-chain surfactant, $[(C_7F_{15})(C_7H_{15})CHSO_4^-Na^+]$. Recently, by molecular dynamics simulation, Salaniwal *et al.* [21] studied the self-assembly of the same surfactant at the same thermodynamic state as Eastoe's work. However, the perfluoroalkane surfactant used in Eastoe's system is not thermodynamically stable and it decomposes in water. Therefore, it would be more interesting to study Johnston's and/or Beckman's [19] perfluoropolyether surfactants using molecular simulation. With the development of the general potential model for perfluoroethers proposed in this work, such comparisons are now possible.

While the thermophysical properties (including phase equilibrium and rheology) of hydrocarbons have been extensively examined through molecular simulation and numerous force fields have been proposed in the literature [22–25], simulation studies and force field development for perfluorinated compounds are much less advanced [26, 27]. Previous work for perfluoro compounds has essentially been for perfluoroalkanes, and has focused on modelling the solid phase diagram of polytetrafluoroethylene using explicit atom models to describe the helical nature of the carbon backbone (see, for example, [28–31]). A notable exception is the work of Koike [32] who recently performed molecular dynamics simulations of confined branched and linear perfluoropolyethers using the consistent valence force field [33] potential model. However, this model was developed for the study of proteins and their binding to active sites and has not been tested for phase equilibrium or bulk transport properties.

Generally it is well recognized that the applicability of a potential model or force field lies in its parameterization. Hence, in order to obtain accurate predictions of the thermophysical properties of perfluoroethers from simulation, it is our goal to develop an accurate potential model that is fitted to liquid state thermodynamic properties in addition to *ab initio* calculations. As a first step towards this goal, in earlier work we proposed a potential model for studying the phase behaviour of perfluoromethylpropylether [34]. In this work, we propose a more general united atom model for perfluoroethers, which we show accurately reproduces the available experimental phase equilibrium data. In addition, Gibbs–Duhem integration techniques (described in the appendix) were extended and used for simultaneous optimization of potential model parameters for several perfluoroether molecules against their experimental vapour–liquid phase equilibrium data in order to speed up the search for an optimized, transferable, parameter set.

2. Methods

The proposed force field for perfluoroethers consists of bond angle bending terms E_{ba}, a torsional term $E_{torsion}$, and terms to describe the van der Waals, E_{vdW}, and electrostatic interactions E_{es}, with the total energy being given by the sum of these contributions:

$$E = E_{ba} + E_{torsion} + E_{vdW} + E_{es}. \quad (1)$$

In the parameterization of this force field, three different types of calculation were performed, *ab initio* quantum mechanical calculations, classical Gibbs ensemble Monte Carlo (GEMC) simulations [35], and Gibbs–Duhem integration calculations [36].

The *ab initio* calculations were applied to generate the partial charges for the electrostatic potential and to obtain the intramolecular bond bending and torsional potentials. All the *ab initio* calculations were performed exclusively with Gaussian 98® [37]. For geometry optimization, the restricted Hartree–Fock method and the cc-pvdz basis set (RHF/cc-pvdz) was applied. For the single point energy calculations, the second order Møller-Plesset, MP2, method was applied with the same basis set. Brief summaries of the methods used to obtain the torsional potential and partial charges are provided below in section 3. For additional details of how the calculations were performed, the reader is referred to our previous publication [34].

To determine the Lennard-Jones parameters, GEMC simulations were used with long-range corrections applied to both the Lennard-Jones and Coulombic terms. The cutoff distance of 14 Å was used throughout the simulations, and after every successful volume exchange move, the cutoff was checked against the new box length to make sure that it remained smaller than half the box length. For Coulombic terms, interactions outside of the cutoff were described by the reaction field method. For each state point on the phase envelope, 1.5 million simulation cycles were carried out

to equilibrate the system and the statistics were taken over 3 million cycles after equilibrium.

In addition to the Monte Carlo simulations we made use of the Gibbs–Duhem integration technique in order to efficiently optimize the Lennard-Jones parameters. From a single run, the Gibbs–Duhem integration technique can provide information on how the phase envelope depends on each specific Lennard-Jones parameter at a particular state point. The information obtained can thus be used to optimize the Lennard-Jones parameters more efficiently.

3. Results and discussion

Owing to the limited experimental data in the open literature on the physical properties of perfluoroethers only three perfluoroethers, for which phase equilibrium data are available, have been used in the potential model development. The molecules are perfluoroethylmethylether (CF_3–O–CF_2–CF_3), perfluoromethylpropylether (CF_3–O–CF_2–CF_2–CF_3), and perfluorodimethoxymethane (CF_3–O–CF_2–O–CF_3) as shown in figure 1. From the study of these three molecules we propose a general united atom parameter set suitable for modelling short perfluoroether molecules.

3.1. *Geometry optimization*

The optimized geometries of the perfluoro compounds such as perfluoroalkanes and perfluoroethers are usually quite different from those of their hydrogenated counterparts because of the replacement of the small hydrogen atoms by the bulky fluorine atoms. The structures of perfluoroethers are further complicated by the fact that the O–C bond length at ~1.36 Å is shorter than that of the C–C bond length of ~1.536 Å and the size of the oxygen group is smaller than that of the CF_x group.

The dihedral angle C–C–O–C for perfluoroethylmethylether is found to have a minimum energy at −162.48°, which, unlike its counterpart in hydrogenated alkanes/ethers, is less than 180° because of the steric hindrance caused by the large fluorine atoms. For perfluoromethylpropylether there are two types of dihedral angle, C–C–C–O and C–C–O–C. The lowest energy value for the C–C–C–O dihedral angle is at almost 180° (177.35°), while the C–C–O–C dihedral angle has a minimum energy value at −161.97°, which is very similar to the C–C–O–C dihedral angle in the shorter perfluoroethylmethylether. Later in this section, we show that these two dihedral angles also have similar energy profiles along the rotation of each angle, suggesting that the atoms associated with these two angles adjust similarly to the rotation, and hence promoting the transferability of the bonded terms of the potential model.

The effect of the shorter C–O bonds on the dihedral angles can be seen most obviously in perfluorodimethoxymethane. The optimized structure has two C–O–C–O dihedral angles at 46.72° and −163.31°, respectively. This shows that the structural distortion at the optimized position is not solely due to the 1–4 interactions along the backbone but is also from the interactions between fluorine atoms on the 1–3 backbone

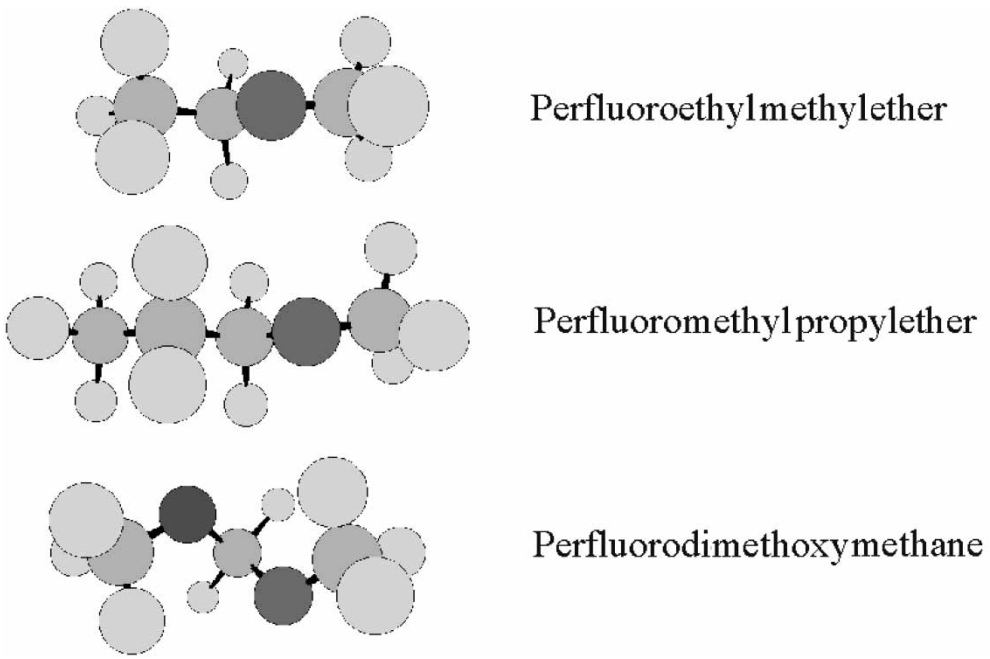

Figure 1. Diagrams of the perfluoroether molecules studied in this work.

Table 1. Optimized geometry parameters.

	Molecule[a]		
	PFEME	PFMPE	PFDMM
Bond lengths (Å)			
C–C	1.529	1.536	
C–O	1.360	1.359	1.358
Bond angles (°)			
C–C–O	107.61	106.72	
C–O-C	121.40	121.39	121.79
C–C–C		115.47	
O–C–O			109.66
Dihedral angles[b](°)			
C–C–O-C	−162.48	−161.97	
C–C–C–O		−177.35	
C–O-C–O 1[c]			46.72
C–O-C–O 2[c]			−163.31

[a] PFEME, perfluoroethylmethylether; PFMPE, perfluoromethylpropylether; PFDMM, perfluorodimethoxymethane.
[b] The 0° angle is designed at the position where the 1–4 sites eclipse each other.
[c] The two C–O–C–O dihedral angles have different values at the optimized structure as mentioned in the text.

sites, because *both* of the 1–4 backbone interactions in this molecule are CF_3–O interactions and would not have the steric interaction that occurs in the CF_3–CF_2 interactions in dihedral angle, C–C–O–C.

To summarize the geometry optimization, table 1 lists the bond lengths, bond angles, and dihedral angles of the optimized structure for each molecule. From these a generalized set of parameters for bond lengths and bond angles has been adopted in this model. This parameter set is listed in table 2.

3.2. *Dihedral energy profile and torsional potential*

Unlike the bond stretching and bending motions which are considered fast intramolecular motions, the torsional motion has a low frequency; therefore, the torsional potential terms are considerably more important than bond stretching and bending terms for molecular simulations. In this work, partial geometry optimizations were performed for each dihedral angle in each molecule and the MP2 method was used to obtain the energy at each of the different conformations in order to generate the energy profile. The torsional potential for each torsional rotation motion has then been obtained by fitting a particular function to the energy profile.

For perfluoromethylpropylether, the energy profiles for the two different dihedral angles, C–C–C–O and C–C–O–C, were presented in previous work [34]. Following the same procedure, perfluoroethylmethylether is represented by four interaction sites in the potential model and so has only one type of dihedral angle, C–C–O–C. The same dihedral angle also occurs in perfluoromethylpropylether. For the ultimate utility of the force field, it is very important for the torsional potential of a particular dihedral angle to be the same no matter which molecule it appears in (i.e., it must be 'transferable') or the potential model will not be reliable when extended to larger molecules. To verify that the torsional potential for C–C–O–C is transferable, the energy profile along the dihedral rotation of perfluoroethylmethylether has been generated with the RHF method, and the result is compared to that of perfluoromethylpropylether obtained with the same method (figure 2). From the figure we see that the two energy profiles closely resemble each other. Therefore, the torsional potential for dihedral angle C–C–O–C in perfluoroethylmethylether has been used for the same dihedral angle in perfluoromethylpropylether and has not been generated separately.

Figure 3 shows the energy profiles obtained from both the RHF and MP2 methods and the torsional potential fitted to the MP2 results for dihedral angle C–O–C–O in perfluorodimethoxymethane. From the figure, one can see that there are two minima, which agree with the two optimized C–O–C–O dihedral angles at −163.31° and 46.72°, respectively. The energy profile changes very rapidly around 163°, and consequently the fitted torsional potential could not reproduce the fine details of the potential.

The C–O–C–O torsional potential is very complex and might appear to suggest that the introduction of oxygen atoms does not make the dihedral angle more flexible, which is contrary to common understanding [11]. Figure 4 shows the comparison of the three energy profiles along the corresponding dihedral angles. From the comparison, it is clear that the energy barrier in the C–O–C–O dihedral angle is indeed the lowest; hence, the introduction of more oxygen atoms does make the dihedral angle more flexible. Another interesting point that can be drawn from the comparison is that the shapes of the C–C–O–C and C–O–C–O energy profiles are similar between 120° and 180°, which confirms that the distortion within this region is caused by the interaction between the fluorine atoms on the 1 and 3 carbon sites, C–O–C.

All the torsional potential models have been fitted to seventh-order polynomials in $\cos(\phi)$ and the results are listed in table 2.

3.3. *Partial charges*

To account for long-range electrostatic interactions, point charges and/or dipoles are typically introduced into the potential model located at atomic centres (or at the centres of sites in the case of united atom potentials).

Table 2. Parameters of the general potential model for perfluoroethers.

Potential	Model	Parameters
Stretching	Fixed	C–C 1.536 Å C–O 1.360 Å
Bending	$E_{ba} = \sum_{angles} K_\theta(\theta - \theta_{eq})^2$	θ_{eq} (°): C–C–C 116.71 C–C–O 109.13 C–O–C 121.69 O–C–O 108.61 K_θ (kJ mol^{-1} rad^{-2}): C–C–C 428.32 C–C–O 455.89 C–O–C 281.38 O–C–O 806.65
Torsional	$E_{torsion} = \sum_{D_i} \sum_{i=0}^{7} a_i \cos^i(\phi)$	C–C–C–O (kJ mol^{-1}): $a_0 = 6.5728$ $a_1 = -22.891$ $a_2 = 10.802$ $a_3 = 22.665$ $a_4 = -26.185$ $a_5 = 15.312$ $a_6 = 17.718$ $a_7 = -7.0944$ C–C–O–C (kJ mol^{-1}): $a_0 = 8.4719$ $a_1 = 9.9988$ $a_2 = -12.342$ $a_3 = -49.346$ $a_4 = 21.799$ $a_5 = 111.320$ $a_6 = -3.3242$ $a_7 = -59.017$ C–O–C–O (kJ mol^{-1}): $a_0 = 2.0217$ $a_1 = -4.5680$ $a_2 = 23.512$ $a_3 = -24.087$ $a_4 = -62.659$ $a_5 = 66.910$ $a_6 = 42.541$ $a_7 = -35.266$
Partial charge (A.U.)[a]	$E_{es} = \frac{1}{4\pi\varepsilon_0}\frac{\overline{q_i q_j}}{r}$	C – C – C – O – C 0.08 −0.11 0.20 −0.42 0.25 C – C – O – C 0.05 −0.13 0.42 −0.24 C – O – C – O – C 0.24 −0.48 0.48 −0.48 0.24
Lennard-Jones	$E_{vdW} = 4\varepsilon\left[\left(\frac{\sigma}{r}\right)^{12} - \left(\frac{\sigma}{r}\right)^{6}\right]$	σ (Å): CF_2 4.6 CF_3 4.6 O 3.0698 CF_2[b] 4.45 CF_2[c] 5.0 ε/k(K): CF_2 30 CF_3 79 O 125 CF_2[b] 30 CF_2[c] 2.5

[a] Generalized partial charge set suggested for long-chain perfluoroethers(not tested):
CF_3 – CF_2 CF_x – O – CF_x
0.08 −0.08 0.24 −0.48 0.24
For long-chain perfluoroethers, only the CF_x sites next to the end or at the end and those next to oxygen are assigned partial charges. The rest are zero charged as in perfluoroalkanes with the net partial charge on a particular site being the sum of all the contributions.

[b] CF_2 site next to one oxygen atom.

[c] CF_2 site surrounded by two oxygen atoms.

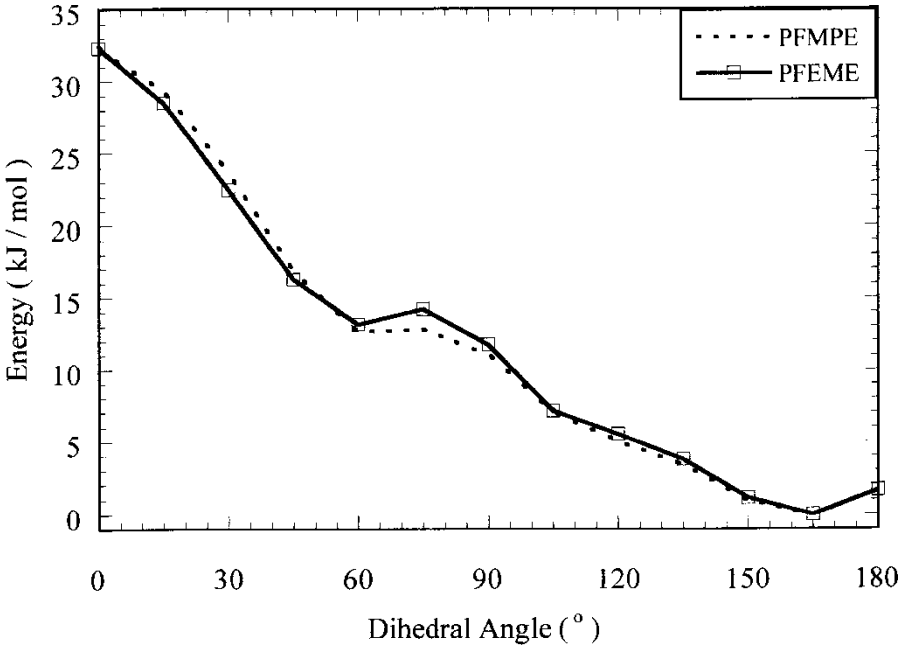

Figure 2. Comparison of the energy profiles of dihedral angle C–C–O–C in perfluoromethylpropylether and perfluoroethylmethylether.

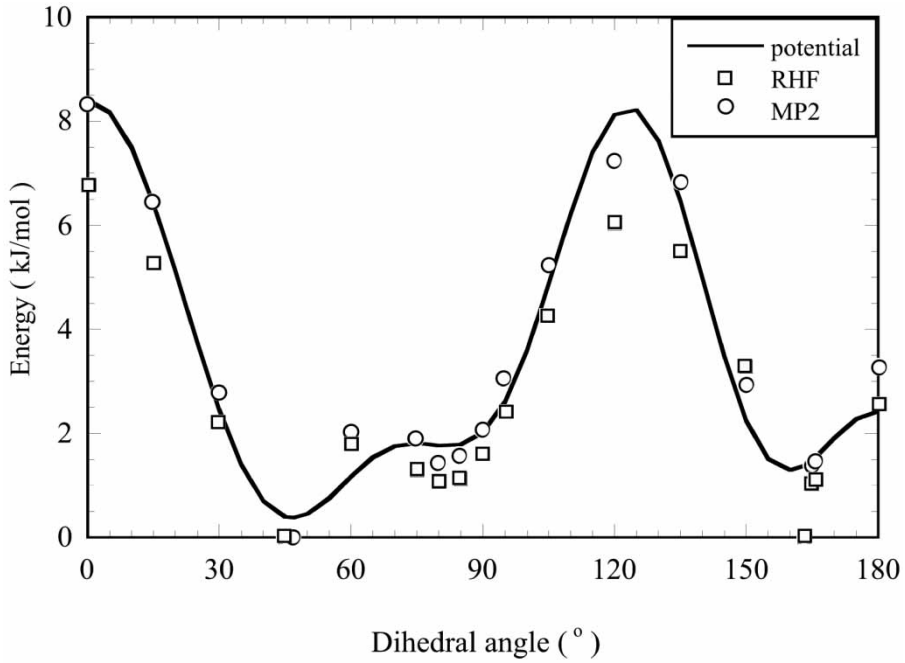

Figure 3. Energy profiles of dihedral angle C–O–C–O in perfluorodimethoxymethane.

In this work, point charges on each site have been used to represent the electrostatic interactions. They were obtained by fitting them to reproduce the *ab initio* electrostatic potential surface. Since the partial charges are dependent on the molecular geometry, they are weighted over multiple conformations using Boltzmann statistics. For additional details, the reader is referred to our previous publication [34].

Adopting partial charges different from the optimal values for each molecule, which is typically done to generate a general and transferable potential model, will cause distortion in the electrostatic interactions and

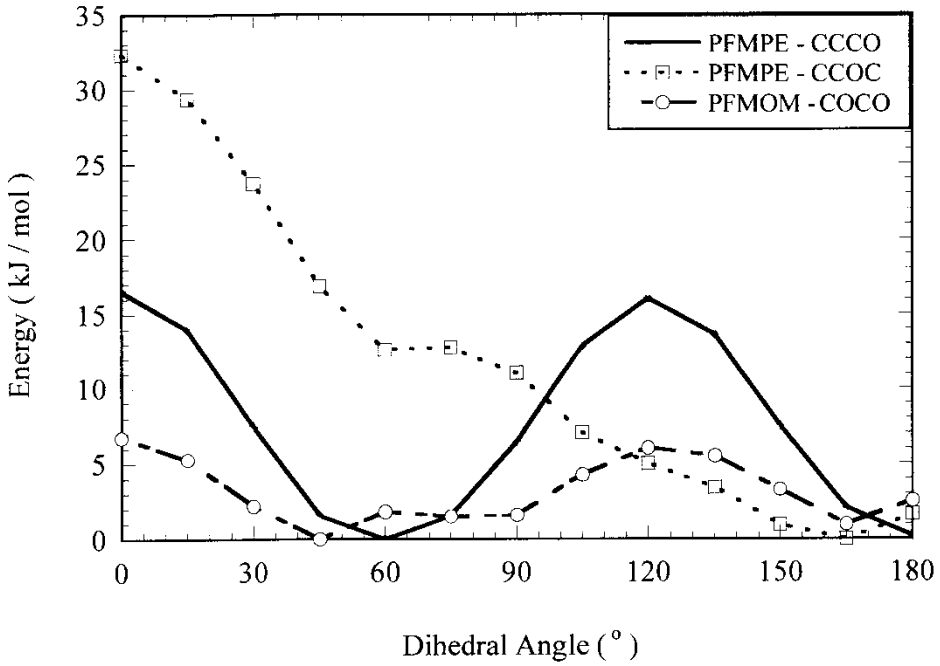

Figure 4. Comparison of the energy profiles of all three dihedral angles found in the studied perfluoroether molecules.

hence jeopardize the validity of the Lennard-Jones parameters determined later. Therefore, partial charges fitted specifically to each molecule have been adopted here and are also suggested for other short perfluoroethers. Later in this section, a set of partial charges generalized for long-chain molecules will be suggested. However, they need to be tested once additional experimental data become available.

3.4. *Fitting Lennard-Jones parameters to phase diagrams*

The search for Lennard-Jones parameters for the united atoms in the modelled perfluoroethers started with the perfluoromethylpropylether molecule because it contains all the Lennard-Jones parameters needed for the shorter perfluoroethylmethylether. To maintain the transferability of the Lennard-Jones parameters from perfluoroalkanes to perfluoroethers, initially the values for the CF_x parameters from the perfluoroalkane potential model proposed in earlier work were used [26]. The optimization from this basis done in previous work [34] led to a set of parameters for oxygen with $\sigma_0 = 3.0698\,\text{Å}$ and $\varepsilon_0/k = 125\,\text{K}$, where k is the Boltzmann constant. This Lennard-Jones parameter set will subsequently be referred to as the 'initial' parameter set, which is shown to reproduce the phase envelope and the critical properties of perfluoromethylpropylether reasonably well. Figure 5 shows the comparison of the phase envelope from the simulation with the initial parameter set and that from experiment for perfluoroethylmethylether. The phase envelope from the simulations is close to the experimental result, which suggests that the Lennard-Jones parameters for oxygen obtained by fitting to the experimental data of perfluoromethylpropylether are adequate. However, the effort to apply the same parameter set to perfluorodimethoxymethane failed, as might be anticipated since the introduction of two oxygen atoms would be expected to affect the Lennard-Jones parameters of the central CF_2 in CF_3–O–CF_2–O–CF_3. To address this problem, the Lennard-Jones parameters for the CF_x site next to oxygen were optimized.

The re-parameterization started with fitting the parameters for perfluoromethylpropylether and perfluoroethylmethylether simultaneously using the Gibbs–Duhem integration technique introduced by Kofke [38]. There are two major simplifications invoked in the application of the Gibbs–Duhem integration technique in this work. The first is that the calculation of the dependence of the phase envelope on the Lennard-Jones parameters is only performed at a single temperature (the effect of this simplification is discussed in the appendix). The second is that the new parameters generated from the technique are obtained by shifting only the liquid branch of the simulated phase envelope to the experimental rather than the whole phase envelope. Because of these two simplifications, the technique could only guide us to the new parameter set, as it did not perform well in the fine-tuning of the parameters. Therefore, at the stage of optimizing the parameters for perfluoromethylpropylether and

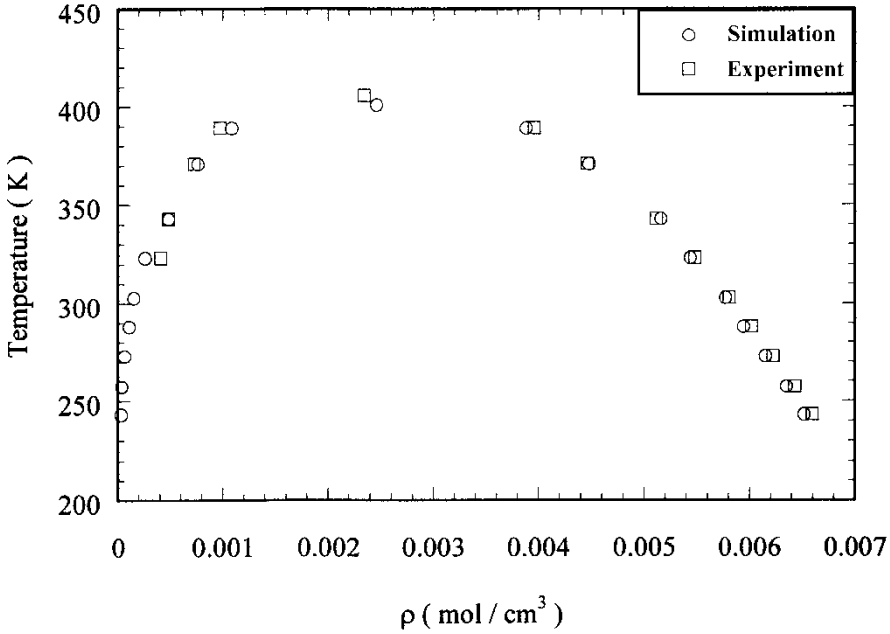

Figure 5. Phase diagram of perfluoroethylmethylether from simulation with the initial parameter set and experiment [40].

perfluoroethylmethylether where only fine-tuning is required, the Gibbs–Duhem technique did not work well and hence was not used. This situation could be improved by carrying out the calculation of the phase envelope dependence at more state points, as explained in the appendix.

Without the Gibbs–Duhem integration technique, the final set of Lennard-Jones parameters for perfluoromethylpropylether and perfluoroethylmethylether was obtained by trial and error [34]. Since the initial parameter set performs well for these two molecules, it was fortunately not necessary to change many parameters. At the end of the optimization process, only the σ of CF_2 adjacent to the oxygen was changed by reducing it to 4.45 Å. This is not unreasonable since the introduction of the oxygen atom reduces the steric hindrance and allows the CF_2 group to adjust to the interaction from the approaching site and hence the CF_2 group shows a smaller apparent size parameter. It is also reasonable that the σ of CF_3 remains unchanged because CF_3 is the end group and without the hindrance from one side, it should be flexible enough whether the oxygen is introduced or not. Figures 6 and 7 show the comparison of the simulated and experimental phase envelopes for perfluoromethylpropylether and perfluoroethylmethylether, respectively, with the final parameter set. Although the final parameter set does not improve the agreement between experiment and simulation for perfluoroethylmethylether, it does result in improvement for perfluoromethylpropylether especially for the critical properties.

With the parameters of CF_3 fixed and unchanged after the optimization process for perfluoroethylmethylether and perfluoromethylpropylether, the σ and ε/k parameters for the central CF_2 site were the only adjustable parameters during the parameter optimization for perfluorodimethoxymethane. With the original parameters for the CF_2 site, the simulation severely overestimated the saturated liquid densities. The Gibbs–Duhem integration technique was again applied to provide a new set of parameters for the CF_2 site and the parameters were quickly adjusted from 4.6 Å and 30 K to 5.36 Å and 24 K for σ and ε/k, respectively. This optimization process is particularly difficult and a variety of combinations of σ and ε/k showed similar performance on the phase envelope, indicating strong cross-correlation between the two parameters. For example, at a temperature of 302 K, with σ and ε/k equal to 5.6 Å and 18 K, the simulated saturated densities are 0.006 20 (mol cm^{-3}) and 0.000 15 (mol cm^{-3}) for the liquid and vapor phases, respectively, which are only slightly different from the values of the final optimized set (0.006 40 (mol cm^{-3}) and 0.000 17 (mol cm^{-3})). This shows that the Gibbs–Duhem integration technique without further modification can determine the correct direction and magnitude of change to reach the optimized parameters.

As previously mentioned, there is a wide choice of parameters for the central CF_2 group in CF_3–O–CF_2–O–CF_3 ranging from a very large ε and a moderately small ε/k to a relatively large σ and a very small ε/k. One possible explanation for this cross-correlation is that the

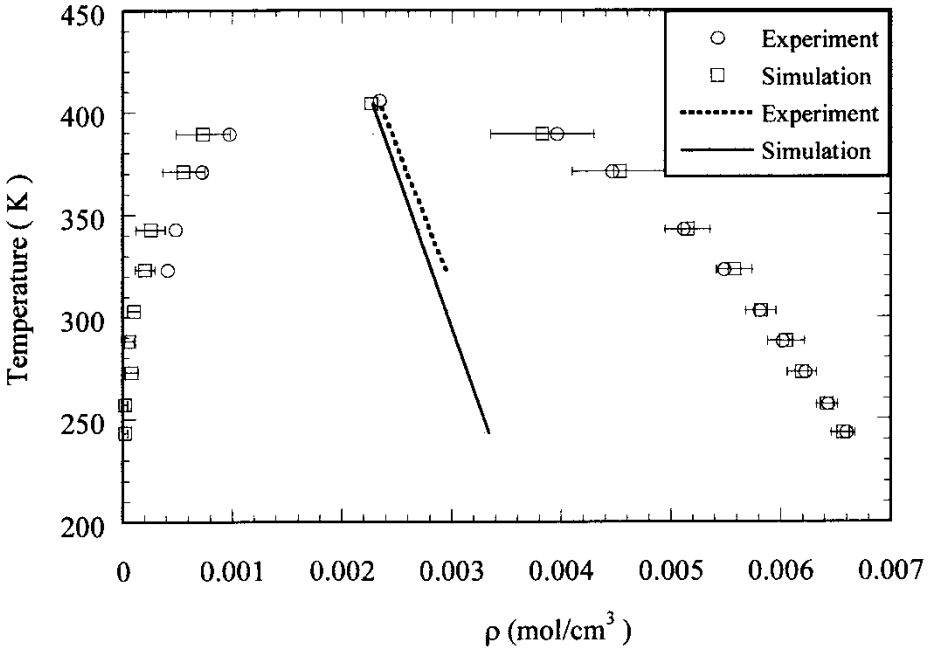

Figure 6. Phase diagram of perfluoromethylpropylether from simulation with the final parameter set and experiment [40]. The solid and dotted lines are the rectilinear lines from simulation and experiment, respectively.

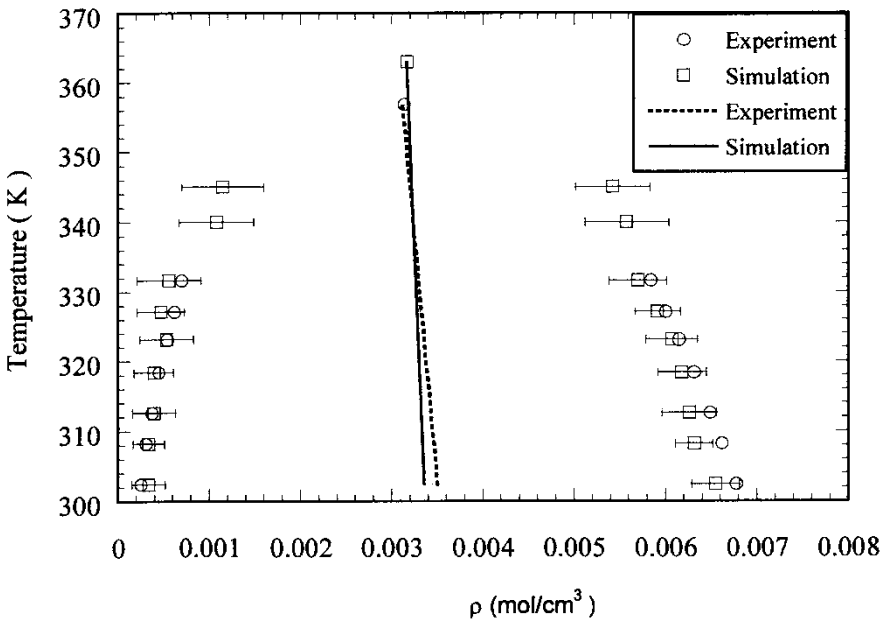

Figure 7. Phase diagram of perfluoroethylmethylether from simulation with the final parameter set and experiment [39]. The solid and dotted lines are the rectilinear lines from simulation and experiment, respectively.

long-ranged interaction with the CF_2 site is mostly accounted for by the electrostatic potential (the partial charge on the CF_2 between two oxygen atoms has a relatively high value at $-0.48e$ compared to other CF_x groups) and the short-range repulsive interaction of this central site is shielded by the O–CF_3 groups on either side. Therefore, a combination of a small ε/k and a comparably smaller σ seems appropriate, and hence the parameters have been chosen to be 5.0 Å and 2.5 K.

Figure 8 shows the comparison of the phase diagram for perfluorodimethoxymethane obtained from experiment and from simulation with the final parameter set. This parameter set does well on the vapour branch of the phase envelope. On the liquid side, it does well at

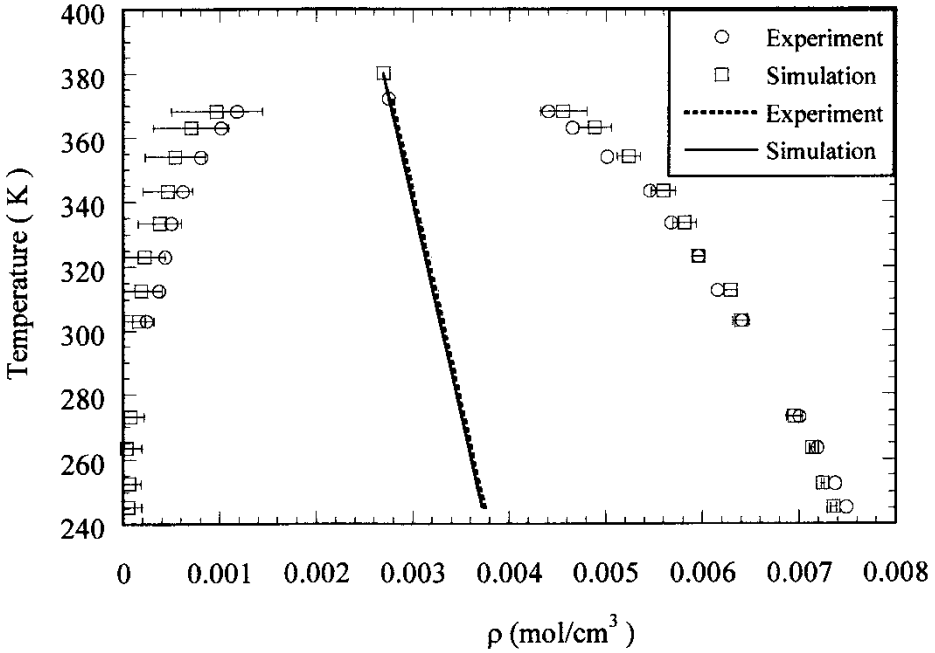

Figure 8. Phase diagram of perfluorodimethoxymethane from simulation with the final parameter set and experiment [40, 41]. The solid and dotted lines are the rectilinear lines from simulation and experiment, respectively.

mid-temperature, underestimates the densities at low temperature, and overestimates at high temperature. Hence, the critical temperature is also overestimated and critical density is underestimated.

An additional test of the utility of the proposed model is to calculate the vapour pressure to compare with experiment. Preliminary calculations of the vapour pressure of perfluoromethylpropylether and perfluorodimethoxymethane yield overestimates of the experimental vapour pressure (20% or more, depending on the molecule and the state condition). This is not surprising since potentials optimized on phase equilibria alone rarely, if ever, result in accurate predictions of the vapour pressure. In order to obtain the vapour pressure accurately, it must be included in the fitting process [39]. However, the results are within reasonable range, and the model does predict the temperature dependence of vapour pressure, particularly at higher pressure. Table 3 shows the critical properties of the three modelled compounds. The critical temperatures and critical densities listed were not used in fitting the model but were obtained by the scaling law with a critical exponent β of 0.325. From the table, we can see that the critical properties are closely predicted by the model.

Table 2 lists the final parameters for all the potentials including the intramolecular and intermolecular potentials. Note that the partial charges for these small molecules are not generalized, as previously discussed. For long chain molecules we have proposed a generalized set of partial charges based on the results of our calculations for these smaller perfluoroether molecules. However, further testing is needed to determine their validity.

Table 3. Critical properties of the modelled molecules.

	Molecule[a]		
	PFEME	PFMPE	PFDMM
Critical temperature (K)			
Simulation	363.05	404.47	380.14
Experiment	356.85	405.81	372.30
Critical density (mol cm^{-3})			
Simulation	0.0031 68	0.0022 66	0.0026 96
Experiment	0.0031 37	0.0023 43	0.0027 50

[a] PFEME; perfluoroethylmethylether; PFMPE; perfluoromethylpropylether; PFDMM; perfluorodimethoxymethane.

4. Conclusions

A potential model for perfluoroethers based on *ab initio* quantum mechanical calculations and available phase equilibrium data has been developed and shown to reproduce the experimental phase envelopes of three perfluoroethers and the critical properties reasonably well. Parameters for CF_2 and CF_3 groups not adjacent to oxygen (which were previously developed for perfluoroalkanes) have been retained so that the potential model has the greatest transferability and new parameters have been proposed for the new groups

encountered in describing perfluoroethers In addition, a set of generalized partial charges for sites in longer perfluoroethers has been proposed but cannot be tested owing to the absence of experimental data.

During the process, the Gibbs–Duhem integration technique has been extended for simultaneous parameter optimization on several molecules; this technique has been used to speed up the dispersion parameter optimization. From the performance of the Gibbs–Duhem integration technique as implemented in this work, it is concluded that the technique can improve the efficiency of the parameter search at the initial stage; however, at the later fine-tuning stage, it was not as valuable as expected.

This work was supported by the Division of Chemical Sciences, Geosciences, and Biosciences of the US Department of Energy (DOE) at Oak Ridge National Laboratory (ORNL) and through subcontract at the University of Tennessee. ORNL is operated for the DOE by UT-Battelle, LLC, under contract number DE-AC05-00OR22725. Fomblin®, Krytox®, and Gaussian® are registered trademarks of Aussimont USA, Inc., E. I. DuPont de Nemours and Co., and Gaussian, Inc., respectively.

Appendix: Implementation and application of Gibbs–Duhem integration

In this work the Gibbs–Duhem integration technique [36, 38] has been extended for the simultaneous optimization of several interaction parameters of several similar compounds. The case illustrated here and used in this work is for parameters of Lennard-Jones sites in molecular fluids.

For a state function, M, the change of M can be described by the total differential of M as follows:

$$\mathrm{d}M = \frac{\partial M}{\partial a_1}\mathrm{d}a_1 + \frac{\partial M}{\partial a_2}\mathrm{d}a_2 + \cdots \tag{A 1}$$

where a_i stands for a set of independent variables and $M = M(a_1, a_2, \ldots)$.

For a thermodynamic system, the change of total Gibbs free energy, $nG = nG(P, T, s, n_1, n_2 \ldots)$, can be expressed as:

$$\mathrm{d}nG = \left(\frac{\partial nG}{\partial T}\right)\mathrm{d}T + \left(\frac{\partial nG}{\partial P}\right)\mathrm{d}P + \sum\left(\frac{\partial nG}{\partial n_i}\right)\mathrm{d}n_i + \left(\frac{\partial nG}{\partial s}\right)\mathrm{d}s \tag{A 2}$$

where s is a particular independent variable other than temperature T, pressure P, and number of moles n_i, of each component. The partial differentiation is only with respect to the corresponding independent variable, with the other variables being held constant.

From fundamental thermodynamics,

$$nG = \sum n_i\mu_i \tag{A 3}$$

where μ is the chemical potential. The total differentiation of equation (A3) gives:

$$\mathrm{d}nG = \sum(n_i\,\mathrm{d}\mu_i + \mu_i\,\mathrm{d}n_i). \tag{A 4}$$

Combining equations (A2) and (A4) and applying to pure fluid, one has:

$$n\,\mathrm{d}\mu = \left(\frac{\partial nG}{\partial T}\right)\mathrm{d}T + \left(\frac{\partial nG}{\partial P}\right)\mathrm{d}P + \left(\frac{\partial nG}{\partial s}\right)\mathrm{d}s. \tag{A 5}$$

Note that this is just the Gibbs–Duhem equation for a pure fluid with an additional independent variable. If one is interested in the correlation between P and T, then equation (A 5) will lead to the basic equation for Gibbs–Duhem integration, the Clapeyron equation.

Now, assuming that one is interested in the correlation between T and s as an independent variable for the potential energy, and keeping P and n constant:

$$\mathrm{d}\mu = \left(\frac{\partial G}{\partial T}\right)\mathrm{d}T + \frac{1}{n}\left(\frac{\partial nG}{\partial s}\right)\mathrm{d}s \tag{A 6}$$

in which,

$$\left(\frac{\partial G}{\partial T}\right)_{P,n,s\ldots} = -S \tag{A 7}$$

assuming nG can be given as $\beta nG = -\ln Q$ where Q is the partition function; in this case $Q = \int \exp[-\beta U(s)]$. Then, one has

$$\left(\frac{\partial \beta nG}{\partial s}\right) = -\frac{1}{Q}\frac{\partial Q}{\partial s} = \left\langle\frac{\partial(\beta U)}{\partial s}\right\rangle. \tag{A 8}$$

Let $D_s = (1/n)(\partial nG/\partial s)$ and write down the equation for two phases:

$$\mathrm{d}\mu_\alpha = -S_\alpha\mathrm{d}T + D_{s\alpha}\mathrm{d}s, \tag{A 9}$$

$$\mathrm{d}\mu_\beta = -S_\beta\mathrm{d}T + D_{s\beta}\mathrm{d}s. \tag{A 10}$$

Along the equilibrium line, $\mathrm{d}\mu_\alpha$ should be equal to $\mathrm{d}\mu_\beta$; therefore

$$-S_\alpha\,\mathrm{d}T + D_{s\alpha}\,\mathrm{d}s = -S_\beta\,\mathrm{d}T + D_{s\beta}\,\mathrm{d}s. \tag{A 11}$$

Rearranging equation (A 11) gives:

$$\left(\frac{\mathrm{d}T}{\mathrm{d}s}\right)_{\text{eq.}} = \frac{\Delta D_s}{\Delta S}. \tag{A 12}$$

For a reversible process such as an equilibrium phase transition, $\Delta S = \Delta H/T$, and equation (A 12) becomes:

$$\left(\frac{\mathrm{d}T}{\mathrm{d}s}\right)_{\text{eq.}} = \frac{\Delta D_s}{\Delta H/T}. \tag{A 13}$$

Now, D_s is needed. For the Lennard-Jones pair potential

$$U = \frac{1}{2}\sum_i \sum_{j\neq i} \sum_m \sum_n 4\varepsilon_{mn}\left[\left(\frac{\sigma_{mn}}{r}\right)^{12} - \left(\frac{\sigma_{mn}}{r}\right)^{6}\right]\text{inter} + \frac{1}{2}\sum_i \sum_m \sum_{|m-n|\geq 4} 4\varepsilon_{mn}\left[\left(\frac{\sigma_{mn}}{r}\right)^{12} - \left(\frac{\sigma_{mn}}{r}\right)^{6}\right]\text{intra}. \tag{A 14}$$

Note that the potential energy normally contains the contributions from other sources such as the electrostatic potential and bonding potentials such as bending and torsional potentials. However, those interactions are independent of any change in ε and σ; therefore, they are neglected here. Since the summation in equation (A 14) is only important during the code implementation, the focus here is on the potential itself. One needs to know the effect of both ε and σ on the temperature shift.

For a particular energy parameter ε_t

$$\begin{aligned}\frac{\partial U}{\partial \varepsilon_t} &= 4\frac{\partial}{\partial \varepsilon_t}\left\{(\varepsilon_m\varepsilon_n)^{1/2}\left[\left(\frac{\sigma_m^6\sigma_n^6}{r^{12}}\right) - \left(\frac{\sigma_m^3\sigma_n^3}{r^6}\right)\right]\right\} \\ &= 4\times\frac{1}{2}\left\{(\varepsilon_m\varepsilon_n)^{-1/2}\left[\left(\frac{\sigma_m^6\sigma_n^6}{r^{12}}\right) - \left(\frac{\sigma_m^3\sigma_n^3}{r^6}\right)\right]\right\} \\ &\quad\times\left(\varepsilon_m\frac{\partial\varepsilon_n}{\partial\varepsilon_t} + \varepsilon_n\frac{\partial\varepsilon_m}{\partial\varepsilon_t}\right)\left(\frac{\varepsilon_m\varepsilon_n}{\varepsilon_m\varepsilon_n}\right) \\ &= 2\left\{(\varepsilon_m\varepsilon_n)^{1/2}\left[\left(\frac{\sigma_m^6\sigma_n^6}{r^{12}}\right) - \left(\frac{\sigma_m^3\sigma_n^3}{r^6}\right)\right]\right\} \\ &\quad\times\left(\frac{1}{\varepsilon_n}\frac{\partial\varepsilon_n}{\partial\varepsilon_t} + \frac{1}{\varepsilon_m}\frac{\partial\varepsilon_m}{\partial\varepsilon_t}\right)\end{aligned} \tag{A 15}$$

where geometric mean combining rules have been used for $\varepsilon_{mn} = (\varepsilon_m\varepsilon_n)^{1/2}$ and $\sigma_{mn} = (\sigma_m\sigma_n)^{1/2}$. Since reduced units are used in the code, the part of the equation that is calculated in the loop of simulation code needs to be transformed into reduced units:

$$\begin{aligned}\frac{\partial U}{\partial \varepsilon_t} &= 2\left\{\left(\varepsilon_m^*\varepsilon_n^*\right)^{1/2}\left[\left(\frac{\sigma_m^{*6}\sigma_n^{*6}}{r^{*12}}\right) - \left(\frac{\sigma_m^{*3}\sigma_n^{*3}}{r^{*6}}\right)\right]\right\} \\ &\quad\times\varepsilon_{\mathrm{R}}\left(\frac{1}{\varepsilon_n}\frac{\partial\varepsilon_n}{\partial\varepsilon_t} + \frac{1}{\varepsilon_m}\frac{\partial\varepsilon_m}{\partial\varepsilon_t}\right)\end{aligned} \tag{A 16}$$

where ε_{R} is the reference energy parameter.

For a particular size parameter, σ_t:

$$\begin{aligned}\frac{\partial U}{\partial \sigma_t} &= 4\frac{\partial}{\partial \sigma_t}\left\{(\varepsilon_m\varepsilon_n)^{1/2}\left[\left(\frac{\sigma_m^6\sigma_n^6}{r^{12}}\right) - \left(\frac{\sigma_m^3\sigma_n^3}{r^6}\right)\right]\right\} \\ &= 4(\varepsilon_m\varepsilon_n)^{1/2}\frac{\partial}{\partial \sigma_t}\left\{\left[\left(\frac{\sigma_m^6\sigma_n^6}{r^{12}}\right) - \left(\frac{\sigma_m^3\sigma_n^3}{r^6}\right)\right]\right\} \\ &= 4(\varepsilon_m\varepsilon_n)^{1/2}\left\{\begin{array}{l}\left(6\dfrac{\sigma_m^5\sigma_n^6}{r^{12}}\dfrac{\partial\sigma_m}{\partial\sigma_t}\cdot\dfrac{\sigma_m}{\sigma_m} + 6\dfrac{\sigma_m^6\sigma_n^5}{r^{12}}\dfrac{\partial\sigma_n}{\partial\sigma_t}\cdot\dfrac{\sigma_n}{\sigma_n}\right) \\ -\left(3\dfrac{\sigma_m^2\sigma_n^3}{r^6}\dfrac{\partial\sigma_m}{\partial\sigma_t}\cdot\dfrac{\sigma_m}{\sigma_m} + 3\dfrac{\sigma_m^3\sigma_n^2}{r^6}\dfrac{\partial\sigma_n}{\partial\sigma_t}\cdot\dfrac{\sigma_n}{\sigma_n}\right)\end{array}\right\} \\ &= 4(\varepsilon_m\varepsilon_n)^{1/2}\left\{\begin{array}{l}\left(6\dfrac{\sigma_m^6\sigma_n^6}{r^{12}}\dfrac{\partial\sigma_m}{\sigma_m\partial\sigma_t} + 6\dfrac{\sigma_m^6\sigma_n^6}{r^{12}}\dfrac{\partial\sigma_n}{\sigma_n\partial\sigma_t}\right) \\ -\left(3\dfrac{\sigma_m^3\sigma_n^3}{r^6}\dfrac{\partial\sigma_m}{\sigma_m\partial\sigma_t} + 3\dfrac{\sigma_m^3\sigma_n^3}{r^6}\dfrac{\partial\sigma_n}{\sigma_n\partial\sigma_t}\right)\end{array}\right\} \\ &= 4(\varepsilon_m\varepsilon_n)^{1/2}\left\{\left(6\frac{\sigma_m^6\sigma_n^6}{r^{12}}\right) - \left(3\frac{\sigma_m^3\sigma_n^3}{r^6}\right)\right\}\left(\frac{\partial\sigma_m}{\sigma_m\partial\sigma_t} + \frac{\partial\sigma_n}{\sigma_n\partial\sigma_t}\right).\end{aligned} \tag{A 17}$$

Again, one needs to use reduced units in part of the expression to go with the code:

$$\begin{aligned}\frac{\partial U}{\partial \sigma_t} &= 4\left\{\left(\varepsilon_m^*\varepsilon_n^*\right)^{1/2}\left[6\left(\frac{\sigma_m^{*6}\sigma_n^{*6}}{r^{*12}}\right) - 3\left(\frac{\sigma_m^{*3}\sigma_n^{*3}}{r^{*6}}\right)\right]\right\} \\ &\quad\times\varepsilon_{\mathrm{R}}\left(\frac{\partial\sigma_m}{\sigma_m\partial\sigma_t} + \frac{\partial\sigma_n}{\sigma_n\partial\sigma_t}\right).\end{aligned} \tag{A 18}$$

The calculations can be carried out along with the calculation of the Lennard-Jones interaction energy in the simulation, and then the ensemble average can be taken to give D_s for both phases with respect to different size and energy parameters.

With equations (A 16) and (A 18), the step-by-step procedure to optimize the Lennard-Jones parameters is as follows.

(1) Carry out Gibbs ensemble Monte Carlo simulation with a predetermined set of Lennard-Jones parameters and equations (A16) and (A18) implemented. This should be done at a temperature in the middle of the phase envelope for all compounds if only one set of simulations is planned for each compound. From this ΔD_s at this temperature can be obtained.
(2) Obtain the system pressure and saturated molar volumes for each phase diagram, and hence the ΔH.
(3) Calculate the shift of equilibrium temperature owing to the parameter changes by equation (A 13). A set of optimized parameters can be obtained by adjusting the equilibrium temperature to the experimental phase envelopes for all the compounds.

(4) On the basis of the newly calculated state point from step 3, use regular Gibbs–Duhem integration [38] to obtain the whole phase diagram. If the phase envelope is satisfactory, proceed to step 5. If not, use the set of parameters obtained in step 3 as the pre-selected set of parameters and go back to step 1.

(5) Perform Gibbs ensemble Monte Carlo on each data point on every phase diagram to test the actual performance of the parameter set. In step 1, molecular simulation is carried out only at one equilibrium temperature, and this may be the reason for non-convergence of the procedure if it is encountered. In this case, step 1 needs to be done at several different temperatures along the coexistence line and dT/ds between two designated temperatures should be interpolated. Another possible reason for non-convergence may be the complexity of the contours with respect to the Lennard-Jones parameters. In this case, a limit on the maximum parameter changes in step 3 should be set, and more iterations may be necessary to achieve the final optimized set of parameters.

References

[1] Kroschwitz, J. I., and Howe-Grant, M., 1991, *Encyclopedia of Chemical Technology*, 4th edn, Vol. 11 (New York: Wiley), pp. 499–504.

[2] May, G., 1997, *Chemistry in Britain*, August, pp. 34–36.

[3] Rudnick, L. R., and Shubkin, R. L., 1999, *Synthetic Lubricants and High Performance Functional Fluids*, Chemical Industry Series, Vol. 77 (New York: Marcel Dekker).

[4] Schwartz, M., 1997, *J. Fluorine Chem.*, **83,** 9.

[5] Bartz, W. J., 1992, *Lubrication Engng*, **48,** 765.

[6] Sadeghi, F., Trope, E. J., and Schnell, T. J., 1996, *Tribolol. Transact.*, **39,** 849.

[7] Hamada, T., 2000, *Phys. Chem. chem. Phys.*, **2,** 115.

[8] Ma, X., Gui, J., Smoliar, L., Grannen, K., Marchon, B., Bauer, C. L., and Jhon, M. S., 1999, *Phys. Rev.* E, **59,** 722.

[9] Philips, D. M., and Jhon, M. S., 2002, *J. appl. Phys.*, **91,** 7577.

[10] Izumisawa, S., and Jhon, M. S., *J. appl. Phys.*, **91,** 7583.

[11] Waltman, R. J., 2000, *Chem. Mater.*, **12**, 2039.

[12] Toselli, M., Messori, M., Bongiovanni, R., Malucelli, G., Priola, A., Pilati, F., and Tonelli, C., 2001, *Polymer*, **42,** 1771.

[13] Thanawala, S. K. and Chaudhury, M. K., 2000, *Langmuir*, **16,** 1256.

[14] Bongiovanni, R., Malucelli, G., Pollicino, A., Tonelli, C., Simeone, G., and Priola, A., 1998, *Macromolec. Chem. and Phys.*, **199,** 1099.

[15] Priola, A., Bongiovanni, R., Malucelli, G., Pollicino, A., Tonelli, C., and Simeone, G., 1997, *Macromolec. Chem. and Phys.*, **198,** 1893.

[16] Tonelli, C., Trombetta, T., Scicchitano, M., Simeone, G., and Ajroldi, G., 1996, *J. appl. Polymer Sci.*, **59,** 311.

[17] Cece, A., Jureller, S. H., Kerschner, J. L., and Moschner, K. F., 1996, *J. phys. Chem.*, **100,** 7435.

[18] Johnston, K. P., Harrison, K. L., Clarke, M. J., Howdle, S. M., Heiltz, M. P., Bright, F. V., Carlier, C., and Randolph, T. W., 1996, *Science*, **271,** 624.

[19] Beckman, E. J., 1996, *Science*, **272,** 613.

[20] Eastoe, J., Bayazit, Z., Martel, S., Steytler, D. C., and Heenan, R. K., 1996, *Langmuir*, **12,** 1423.

[21] Salaniwal, S., Cui, S. T., Cummings, P. T., and Cochran, H. D., 1999, *Langmuir*, **15,** 5188.

[22] de Pablo, J. J., 1995, *Fluid Phase Equilibria*, **104,** 195.

[23] Mondello, M., and Grest, G. S., 1995, *J. chem. Phys.*, **103,** 7156.

[24] Nath, S. K., Escobedo, F. A., and de Pablo, J. J., 1998, *J. chem. Phys.*, **108,** 9905.

[25] Errington, J. R., and Panagiotopoulos, A. Z., 1999, *J. phys. Chem.* B, **103,** 6314.

[26] Cui, S. T., Siepmann, J. I., Cochran, H. D., and Cummings, P. T., 1998, *Fluid Phase Equilibria*, **146,** 51.

[27] McCabe, C., Bedrov, D., Smith, G. D., and Cummings, P. T., 2001, *Indust. Engng Chem. Res.*, **40,** 473.

[28] Rothlisberger, U., Laasonen, K., and Klein, M. L., 1996, *J. chem. Phys.*, **104,** 3692.

[29] Holt, D. B., and Farmer, B. L., 1999, *Polymer*, **40,** 4673.

[30] Holt, D. B., and Farmer, B. L., 1999, *Polymer*, **40,** 4667.

[31] Sprik, M., Rothlisberger, U., and Klein, M. L., 1997, *J. phys. Chem.* B, **101,** 2745.

[32] Koike, A., 1999, *J. phys. Chem.*, **103,** 4578.

[33] Dauber-Osguthorpe, P., Roberts, V. A., Osguthorpe, D. J., Genest, M., and Hagler, A. T., 1988, *Proteins: Struct., Funct., Genet.*, **4,** 31.

[34] Li, H.-C., McCabe, C., Cui, S. T., Cummings, P. T., and Cochran, H. D., 2002, *Molec. Phys.*, **100,** 265.

[35] Panagiotopoulos, A. Z., 1987, *Molec. Phy.*, **61,** 813.

[36] Kofke, D. A., 1993, *Molec. Phys.*, **78,** 1331.

[37] Frisch, M. J., Trucks, G. W., Schlegel, H. B., Scuseria, G. E., Robb, M. A., Cheeseman, J. R., Zakrzewski, V. G., Montgomery, J. A. J., Stratmann, R. E., Burant, J. C., Dapprich, S., Millam, J. M., Daniels, A. D., Kudin, K. N., Strain, M. C., Farkas, O., Tomasi, J., Barone, V., Cossi, M., Cammi, R., Mennucci, B., Pomelli, C., Adamo, C., Clifford, S., Ochterski, J., Petersson, G. A., Ayala, P. Y., Cui, Q., Morokuma, K., Malick, D. K., Rabuck, A. D., Raghavachari, K., Foresman, J. B., Cioslowski, J., Ortiz, J. V., Baboul, A. G., Stefanov, B. B., Liu, G., Liashenko, A., Piskorz, P., Komaromi, I., Gomperts, R., Martin, R. L., Fox, D. J., Keith, T., Al-Laham, M. A., Peng, C. Y., Nanayakkara, A., Gonzalez, C., Challacombe, M., Gill, P. M. W., Johnson, B., Chen, W., Wong, M. W., Andres, J. L., Gonzalez, C., Head-Gordon, M., Replogle, E. S., and Pople, J. A., 1998, *Gaussian*, *98* (Pittsburgh PA: Gaussian, Inc).

[38] Kofke, D. A., 1993, *J. chem.. Phys.*, **98,** 4149.

[39] Errington, J. R., and Panagiotopoulos, A. Z., 1999, *J. phys. Chem.* B, **103,** 6314.

[40] Beyerlein, A. L., DesMarteau, D. D., Kul, I., and Zhao, G., 1998, *Fluid Phase Equilibria*, **150–151,** 287.

[41] Salvi-Narkhede, M., Adcock, J. L., Gakh, A., and Van Hook, W. A., 1993, *J. chem. Thermodyn.*, **25,** 643.

[42] Wang, B.-H., Adcock, J. L., Mathur, S. B., and Van Hook, W. A., 1991, *J. chem. Thermodyn*, **23,** 699.